SAND99-2400C

A 3-D SAR approach to IFSAR processing

Armin Doerry[a], Doug Bickel[b]

Sandia National Laboratories
PO Box 5800 MS 0529, Albuquerque, NM 87185-0529

ABSTRACT

Interferometric SAR (IFSAR) can be shown to be a special case of 3-D SAR image formation. In fact, traditional IFSAR processing results in the equivalent of merely a super-resolved, under-sampled, 3-D SAR image. However, when approached as a 3-D SAR problem, a number of IFSAR properties and anomalies are easily explained. For example, IFSAR decorrelation with height is merely ordinary migration in 3-D SAR.

Consequently, treating IFSAR as a 3-D SAR problem allows insight and development of proper motion compensation techniques and image formation operations to facilitate optimal height estimation. Furthermore, multiple antenna phase centers and baselines are easily incorporated into this formulation, providing essentially a sparse array in the elevation dimension.

This paper shows the Polar Format image formation algorithm extended to 3 dimensions, and then proceeds to apply it to the IFSAR collection geometry. This suggests a more optimal reordering of the traditional IFSAR processing steps.

Keywords: IFSAR, Interferometry, Fine Resolution, 3-D, Polar Format

1. INTRODUCTION

Interferometric Synthetic Aperture Radar (IFSAR) is a well known technique whereby typically two SAR images of the same scene, each derived from a slightly different geometry, are compared on the basis of the phase of the resulting pixels to infer pixel height in the otherwise 2-dimensional projection of the scene.[1] The target scene topography extraction is fairly well understood, and a number of IFSAR systems have flown and made impressive 3-dimensional renderings of various target scenes.

The IFSAR process seems to be fairly uniform in the literature. First, two complex SAR images are formed. These are then registered and interfered (phase-compared). The phase difference is then attributed to target height, with resolution of any ambiguities perhaps by some phase-unwrapping process of some kind. The questions remain "Is this process optimal?", "If not, why?", and then "How might it be improved?"

This paper examines an atypical perspective for the collection and processing of IFSAR data, that furthermore suggests some changes in the usual IFSAR processing steps.

a. Correspondence: Email: awdoerr@sandia.gov; WWW: http://www.sandia.gov/radar/sar.html; Telephone: 505/845-8165
b. Correspondence: Email: dlbicke@sandia.gov; Telephone: 505/845-9038

DISCLAIMER

2. BACKGROUND - THE COLLECTION SURFACES IN FOURIER SPACE

Let the IFSAR collection geometry be defined by figure 1. Also consider a radar using a Linear-FM chirp, stretch processing, and quadrature sampling. Neglecting residual video phase errors, the phase of the video signal from an echo of an ideal point target located at **s** can be modeled approximately as

$$\Phi_{video}(i,n,k) \approx \left\{ \frac{4\pi}{c}\left[f_{n,k} + B_{\text{eff},n,k}\left(\frac{i}{I}\right)\right](|\boldsymbol{r}_{c,n,k}| - |\boldsymbol{r}_{c,n,k} - \boldsymbol{s}|) \right\}. \tag{1}$$

i = ADC sampling index ($-I/2 \le i \le I/2-1$),

n = azimuth position index ($-N/2 \le n \le N/2-1$),

k = IFSAR antenna phase center index ($k = 0,1$ for single baseline IFSAR),

$\boldsymbol{r}_{c,n,k}$ = vector from scene center to the effective phase center of the antenna,

$\boldsymbol{s}$ = vector from scene center to the target location,

$f_{n,k}$ = nominal center frequency for the sampled received pulse, and

$B_{\text{eff},n,k}$ = effective bandwidth within the sampled data that determines range resolution. (2)

Note that we will allow center frequency and bandwidth to vary as a function of both pulse number and antenna index. Furthermore, ADC sample times are chosen to track the scene center, that is, such that $i = 0$ after a delay corresponding to the nominal range to the scene center $2|\boldsymbol{r}_{c,n,k}|/c$.

For a target located with x-y-z coordinates (s_x, s_y, s_z), we can expand

$$(|\boldsymbol{r}_{c,n,k}| - |\boldsymbol{r}_{c,n,k} - \boldsymbol{s}|) \approx s_x \cos\psi_{n,k}\sin\alpha_{n,k} - s_y \cos\psi_{n,k}\cos\alpha_{n,k} + s_z \sin\psi_{n,k}. \tag{3}$$

While errors from this approximation need to be dealt with in high-performance IFSAR processing, this approximation is nevertheless adequate to explore motion compensation issues and other IFSAR features.

Within the Fourier space of the target scene, the video samples from a single pulse at a single antenna position describe a linear sequence of samples over a radial segment $(4\pi/c)(f_{n,k} + B_{\text{eff},n,k}\, i/I)$ at polar angles $\alpha_{n,k}$ and $\psi_{n,k}$. This is shown in figure 2. For a single antenna phase center in motion (fixed k), the collection of pulses describe a collection surface in Fourier space. Multiple antenna phase centers (multiple k) describe multiple collection surfaces in the same Fourier space. This is well known and illustrated in figure 3.

The two surfaces define a 3-dimensional volume that is effectively a 3-dimensional aperture in Fourier space.

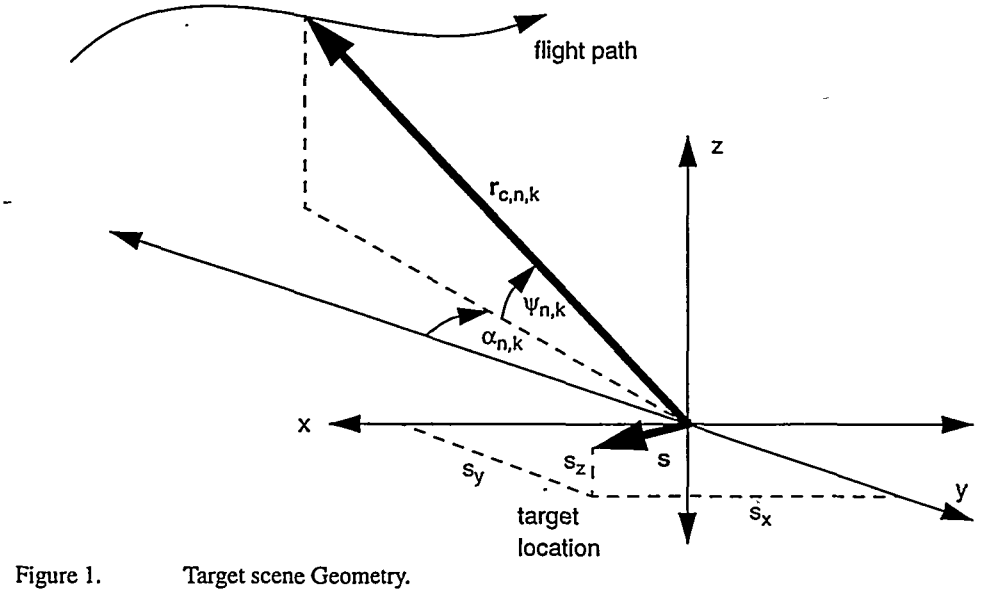

Figure 1. Target scene Geometry.

To facilitate spatial coherence between the two images, each collection surface is typically cropped and resampled such that their projections onto the plane $\omega_z = 0$ is a common region, typically rectangular. A common trapezoidal projection can also be accomplished by pulse-to-pulse adjustment of center frequency *and bandwidth* in the manner

$$f_{n,k} = \kappa_{n,k} f_{0,0}, \text{ and } B_{\text{eff},n,k} = \kappa_{n,k} B_{\text{eff},0,0} \tag{4}$$

where $f_{0,0}$ and $B_{\text{eff},0,0}$ are nominal constant values, and

$$\kappa_{n,k} = \frac{\cos\psi_{0,0}}{\cos\psi_{n,k}\cos\alpha_{n,k}}. \tag{5}$$

This results in the collection surfaces illustrated in figure 4. If azimuth samples are collected in such that

$$\tan\alpha_{n,k} = \tan\alpha_{n,0} = d\alpha\, n \tag{6}$$

for some constant $d\alpha$, then a rectangular projection is achieved merely by a linear resampling in the azimuth direction.

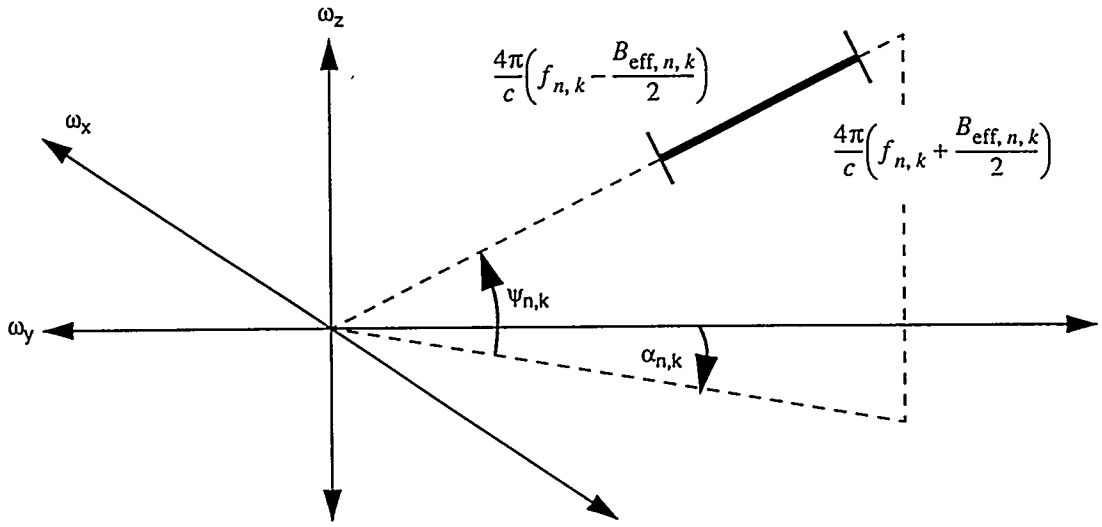

Figure 2. Fourier space of target scene for a single antenna and single pulse.

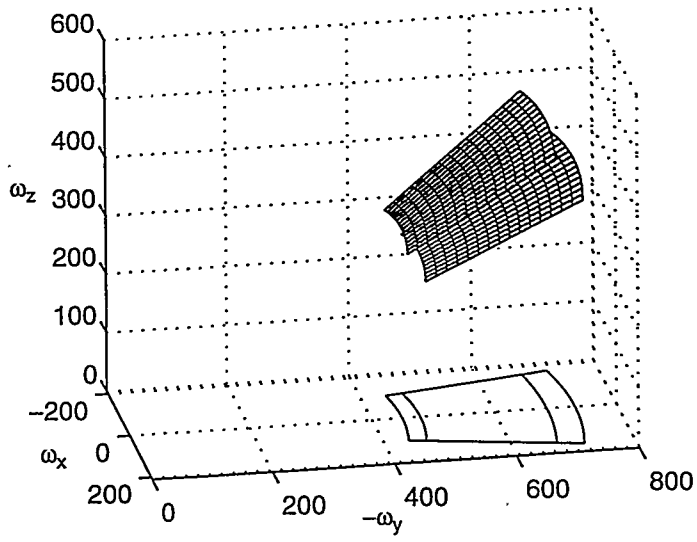

Figure 3. IFSAR collection surfaces in Fourier space, and their projections onto the plane $\omega_z = 0$, for straight-line flight path with broadside squint angle, and with constant waveform parameters.

3. THE DESIRED SURFACES

The ideal 3-d Fourier volume from a processing standpoint is a rectangular parallelepiped (rectangular box) described by independent spatial frequency ranges, or

$$\Phi_{\text{ideal}} = \omega_x s_x + \omega_y s_y + \omega_z s_z \text{ with } \omega_{x_1} \le \omega_x \le \omega_{x_2},\ \omega_{y_1} \le \omega_y \le \omega_{y_2}, \text{ and } \omega_{z_1} \le \omega_z \le \omega_{z_2}. \quad (7)$$

However, the collection volume (after traditional cropping and resampling) looks closer to a more general parallelepiped, as is illustrated in figure 5. While not quite ideal, a non-rectangular parallelepiped is close.

We note that the non-horizontal top and bottom faces indicate a coupling of ω_y and ω_z components, which means that processing parallel to these faces results in measuring a linear sum of s_y and s_z components. This is precisely the range layover effect in SAR images. Nevertheless, processing in the ω_x direction should yield uniquely s_x, and processing in the ω_z direction should yield uniquely s_z. Furthermore, as is well known, once s_z is determined, the layover can be removed to generate a true 3-D rendering, and an ortho-rectified image.

We furthermore note that while nearly so, the two collection surfaces of figure 4 are not, in fact, strictly parallel.

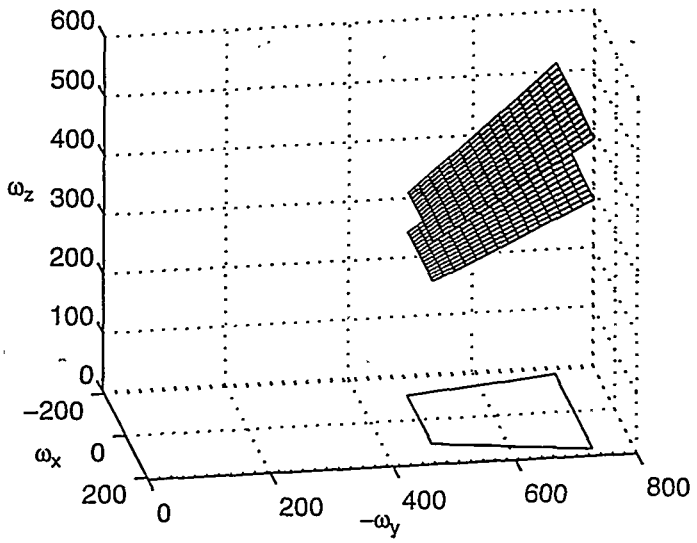

Figure 4. IFSAR collection surfaces in Fourier space, and their projections onto the plane $\omega_z = 0$, for straight-line flight path with broadside squint angle, and with motion-compensated waveform parameters.

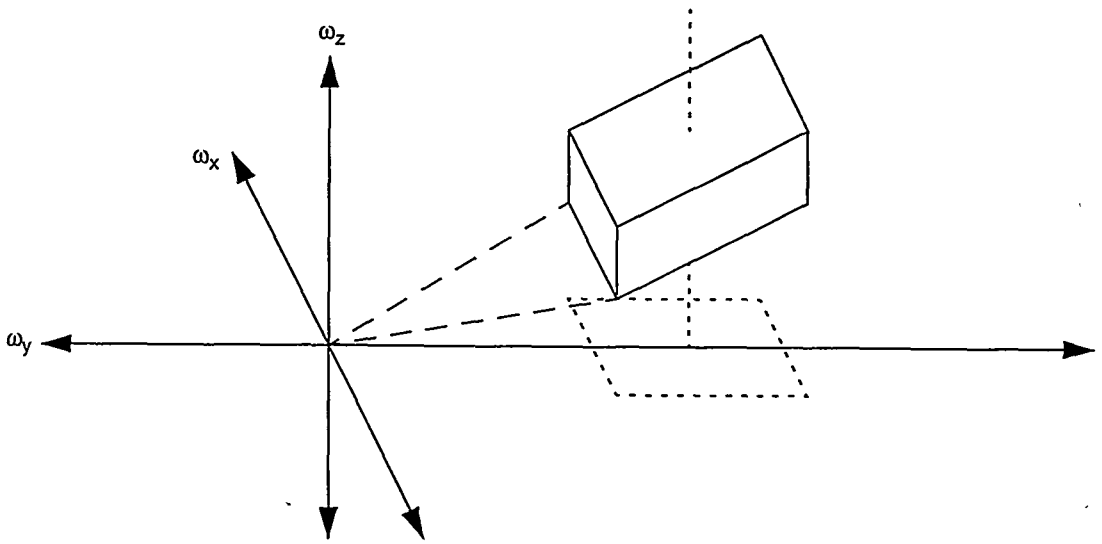

Figure 5. Parallelepiped collection volume in Fourier space of target scene.

4. 3-D PROCESSING - PEAK DETECTION FOR HEIGHT MEASUREMENT

Consider a vertical line passing thru the center of the projection of the parallelepiped onto the $\omega_z = 0$ plane. Let this intersect the collection surfaces where $i = 0$, and $\alpha_{n,k} = 0$. The vertical separation between the two collection surfaces along this line is given by

$$\Delta\omega_z = \frac{4\pi}{\lambda_{0,0}}\cos\psi_{0,0}(\tan\psi_{0,1} - \tan\psi_{0,0}) \approx \frac{4\pi}{\lambda_{0,0}}\left(\frac{\Delta\psi_{0,1}}{\cos\psi_{0,0}}\right) \tag{8}$$

where $\lambda_{0,0} = c/f_{0,0}$ = nominal wavelength, and $\Delta\psi_{0,1} = \psi_{0,1} - \psi_{0,0}$ which is presumed to be small.

We relate the general angular difference $\Delta\psi_{n,k}$ to the baseline length between effective phase centers as

$$\Delta\psi_{n,k} \approx b_\perp / |r_{c,n,0}| \tag{9}$$

where $b_\perp$ is the length of the projection of the actual baseline in the direction of the target scene (perpendicular to $r_{c,n,0}$).

For the parallelepiped of figure 5, the separation $\Delta\omega_z$ would hold even after normal range compression and Doppler compression (i.e. image formation). Between the two images so formed, a DFT across collocated pixels (in the ω_z direction) would yield an impulse response of the general form

$$\frac{\sin(\Delta\omega_z s_z)}{\sin(\Delta\omega_z s_z/2)} \tag{10}$$

with nominal lobe width

$$\rho_z \approx \frac{2\pi}{\Delta\omega_z} = \frac{\lambda_{0,0}}{2(\Delta\psi_{0,1}/\cos\psi_{0,0})}. \tag{11}$$

However, by making the presumption that the target scene manifests itself as a thin reflecting surface, with but a single target height for any location, then we might resolve target height to something with much finer precision than the just-calculated ρ_z. Our ability to super-resolve target height becomes dependent on the Signal-to-Noise (SNR) ratio in the respective pixels. The problem is now one of spectral estimation, or estimating the location of a single spectral peak in noise.

It has been shown that the variance of the location of the spectral peak can be expressed as[2,3]

$$\sigma_z^2 = \frac{1}{\mathrm{SNR}(\Delta\omega_z)^2} = \left(\frac{\lambda_{0,0}}{4\pi}\frac{\cos\psi_{0,0}}{\Delta\psi_{0,1}}\right)^2\left(\frac{1}{\mathrm{SNR}}\right). \tag{12}$$

This expression relates the super-resolved height-noise to SNR, and is identical to the more conventionally derived expression based on phase noise between the two phase centers, recognizing that the Cramer-Rao bound for phase noise variance relates to large SNR by the well-known expression

$$\sigma_\phi^2 = \frac{1}{\mathrm{SNR}}. \tag{13}$$

As a final note, if the ω_z dimension is sampled too coarsely for the target scene content ($\Delta\omega_z$ is too big), then we might expect aliasing in the spatial domain. This is, of course, the phase-ambiguity problem that plagues many IFSARs.

This validates the equivalence of IFSAR to super-resolved, under-sampled, 3-D SAR.

5. 3-D MIGRATION - NON-PARALLEL COLLECTION SURFACES

We recall that the collection surfaces in figure 4 were described by

$$\Phi_{video}(i,n,k) \approx \left\{\frac{4\pi}{c}\left[f_{0,0} + B_{\mathrm{eff},0,0}\left(\frac{i}{I}\right)\right]\cos\psi_{0,0}\left(s_x\tan\alpha_{n,0} - s_y + s_z\frac{\tan\psi_{n,k}}{\cos\alpha_{n,0}}\right)\right\} \tag{14}$$

from which we note that the actual vertical separation between collection surfaces varies depending on the location on the collection surface (indices i and n), and is expressed by

$$\begin{aligned}\Delta\omega_{z,i,n} &= \frac{4\pi}{c}\left[f_{0,0} + B_{\text{eff},0,0}\left(\frac{i}{I}\right)\right]\frac{\cos\psi_{0,0}}{\cos\alpha_{n,0}}(\tan\psi_{n,1} - \tan\psi_{n,0}) \\ &\approx \frac{4\pi}{c}\left[f_{0,0} + B_{\text{eff},0,0}\left(\frac{i}{I}\right)\right]\left(\frac{\cos\psi_{0,0}}{\cos\alpha_{n,0}\cos^2\psi_{n,0}}\right)\frac{b_\perp}{|r_{c,n,0}|} \qquad \text{for } b_\perp \ll |r_{c,n,k}|\end{aligned} \tag{15}$$

This variation of vertical frequency separation (bandwidth) is plotted in figure 6(a) for a Ku-band IFSAR operating at a broadside squint angle with a 1 ft. baseline at 5 km range, 45° depression angle, and 4-inch image resolution. While the dominant change in vertical bandwidth $\Delta\omega_z$ is across the ω_y direction for broadside imaging (with index i), this is not necessarily true for severe squint angles, as is illustrated in figure 6(b). As squint angles become more severe, substantial variation in $\Delta\omega_z$ may occur as a function of azimuth angle $\alpha_{n,k}$.

Ignoring this dependence of spatial frequencies on more than one index value generates migration of spectral peaks as a function of the undesired indices. Consequently, if we form ordinary 2-D images (transforming across indices i and n in the model of equation (14) for each antenna k), then we might expect the location of a scatterer at height s_z to move depending on index k. Eventually, for large enough s_z, this migration will be entirely to an adjacent resolution cell, thereby decorrelating the two images for that particular pixel location. We can expect this effect to be exacerbated at finer resolutions and more severe squint angle.

The dependence on $\alpha_{n,k}$ can be mitigated, even for severe squint angles, by adjusting the baseline projection $b_\perp$ as a function of the pulse-to-pulse geometry. For example, if we force

$$b_\perp \rightarrow b_{\perp,n,1} = b_{\perp,0,1}\cos\alpha_{n,0}\left(\frac{\cos\psi_{n,0}}{\cos\psi_{0,0}}\right)^2\frac{|r_{c,n,0}|}{|r_{c,0,0}|} \tag{16}$$

then it can be verified that $\Delta\omega_{z,i,n} = \Delta\omega_{z,i,0}$ has no further dependence on azimuth angle $\alpha_{n,0}$. With this modification, the collection plane vertical separations of figure 6 become as shown in figure 7, and indicates a substantially stabilized vertical bandwidth, especially with squint angle. One might envision modulating the baseline on a pulse-to-pulse basis via some sort of mechanical baseline adjustment between antenna pairs, or perhaps a phase center adjustment in an electrically programmable phased array. Even a rotation of the true baseline would change the projection length. While adjusting radar frequencies could also stabilize $\Delta\omega_z$, doing so would adversely affect the other dimensions.

Modulating the baseline within a single pulse to flatten $\Delta\omega_z$ across the ω_y direction seems more problematic.

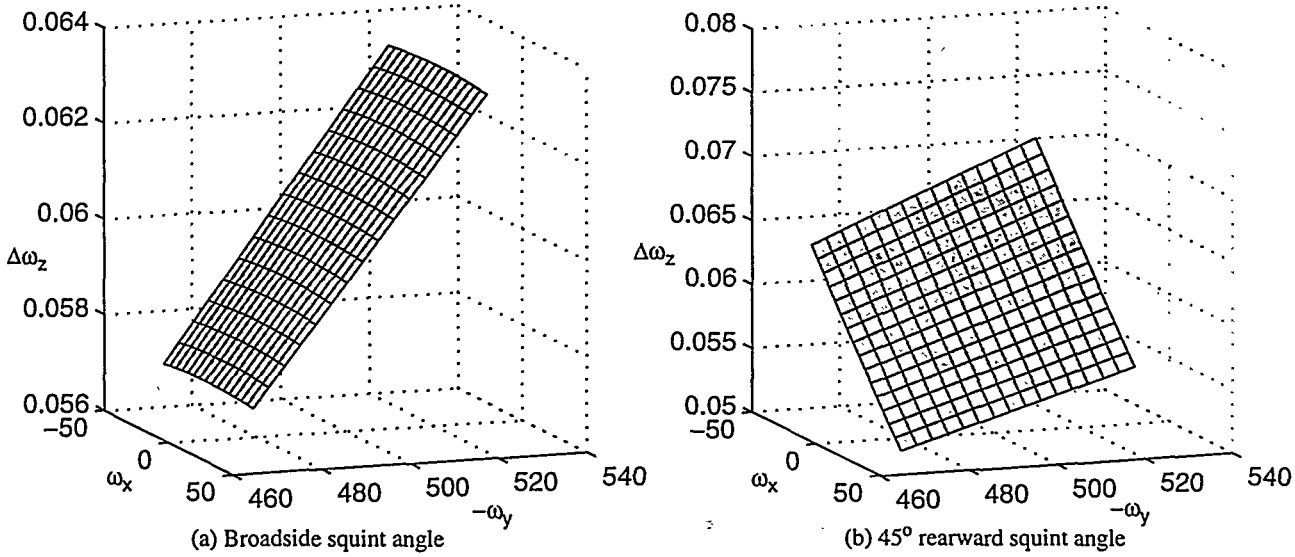

(a) Broadside squint angle

(b) 45° rearward squint angle

Figure 6. Collection plane vertical separation for Ku-band IFSAR with a 1 ft. baseline at 5 km range, 45° depression angle, and 4-inch image resolution.

6. MULTIPLE BASELINE IFSAR

Heretofore we have discussed but a single pair of collection surfaces with a single baseline. Clearly, as is well known, as baseline separation increases ($\Delta\omega_z$ increases), finer vertical resolution (less height noise) is achievable, but at a cost of greater ambiguity due to the undersampling of the target scene. While ever more exotic phase unwrapping algorithms might help this, the more straightforward solution is to add more antenna phase centers at different baseline separations. This increases the number of non-coplanar collection surfaces in Fourier space.

In our models for video phase, this simply allows the antenna index k to be extended, to perhaps $0 \le k \le (K-1)$, where K is the total number of antenna phase centers. Consequently, with proper real-time motion compensation, equation (14) is still valid, but can be further extended to

$$\Phi_{video}(i,n,k) \approx \left\{ \frac{4\pi}{c}\left[f_{0,0} + B_{\text{eff},0,0}\left(\frac{i}{I}\right)\right]\cos\psi_{0,0}\left(\begin{array}{l} s_x \tan\alpha_{n,0} - s_y + s_z \dfrac{\tan\psi_{n,0}}{\cos\alpha_{n,0}} \\ + \dfrac{s_z}{\cos\alpha_{n,0}\cos^2\psi_{n,0}}\left(\dfrac{b_{\perp,n,k}}{|r_{c,n,0}|}\right) \end{array} \right) \right\} \tag{17}$$

where $b_{\perp,n,k}$ is the projected baseline between a reference antenna ($k = 0$) and the effective phase center due to another antenna of interest, with index $k > 1$. Collection surfaces compensated in this manner are illustrated in figure 8.

The natural question is "What are the optimal set of baselines $b_{\perp,n,k}$ for a given number of phase centers K?"

Returning to the 3-D SAR model, this question can be translated to "How should a finite number of array elements be spaced to maximize spatial resolution with minimum ambiguity?" This is, in fact, a well-studied problem in antenna theory that goes by any of several names including "sparse arrays", "thinned arrays", and "aperiodic arrays".[4] In any case, a more in-depth treatment of optimal element placement (and hence optimal baseline selection) is beyond the scope of this paper.

Figure 9 illustrates how additional effective phase centers might help in selecting the proper s_z from an otherwise ambiguous set. It should be noted that since we make the a priori assumption of a single height for every (s_x,s_y) pair, sidelobes in the s_z direction need to be diminished only to the point of achieving proper noise margin.

It has already been established that treating the collection of vertically offset phase centers due to multiple baselines as a single comprehensive set of spatial frequency samples is optimal, although other schemes might offer computational advantages.[5,6]

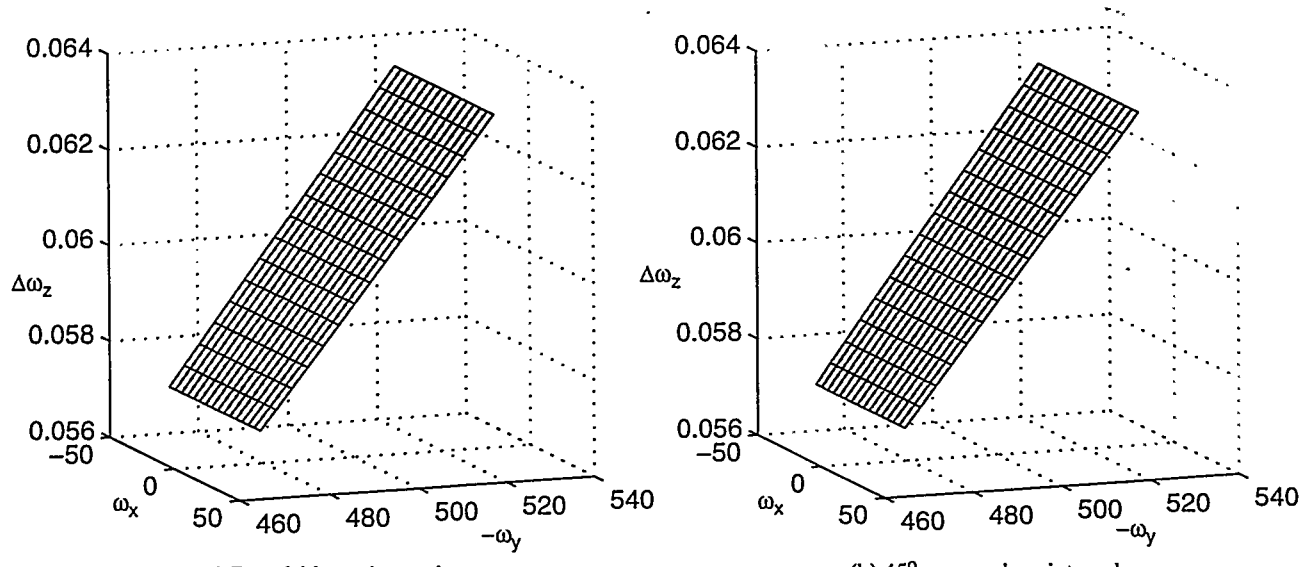

(a) Broadside squint angle

(b) 45° rearward squint angle

Figure 7. Collection plane vertical separation using pulse-to-pulse baseline modulation for Ku-band IFSAR with a 1 ft. baseline at 5 km range, 45° depression angle, and 4-inch image resolution.

7. MODIFIED 3-D POLAR FORMAT PROCESSING

The fundamental principle governing conventional 2-D polar format processing of SAR images is a recognition of the non-rectangular region of projection onto the plane $\omega_z = 0$ for the raw phase history data. For the typical analysis of a constant waveform and constant depression angle, this amounts to a segment of an annular ring. Furthermore, an efficient digital 2-D transform to the spatial domain requires first resampling the Fourier domain data such that their projections are onto a rectangular grid. These steps eliminate the significant migration that would otherwise limit SAR image quality, especially away from the scene center. Furthermore, elements of these resampling steps can often be incorporated into both the real-time motion compensation as previously discussed, and also perhaps into the transform itself.[7]

In a similar manner, an extension of efficient polar format processing to three dimensions would seek to effectively resample the Fourier domain data to the parallelepiped of figure 5, with equally spaced samples parallel to all faces. As with 2-D processing, some of this can be done with proper real-time motion compensation, and some can be done in the course of transforming the data.

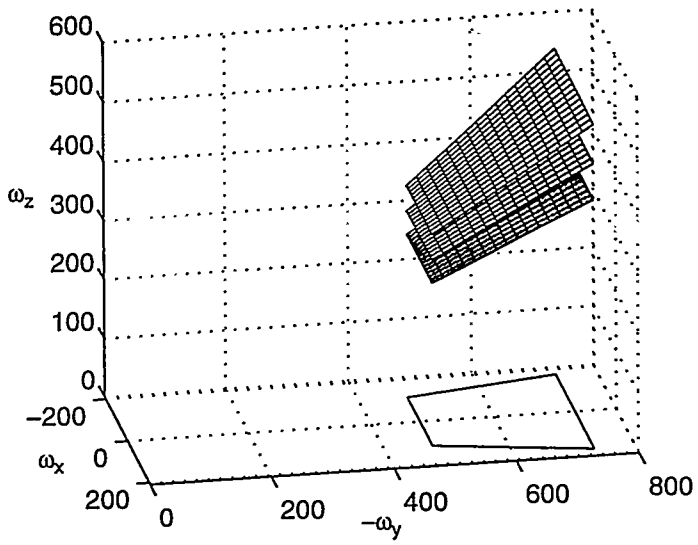

Figure 8. Multiple IFSAR collection surfaces in Fourier space, and their projections onto the plane $\omega_z = 0$, for straight-line flight path with broadside squint angle, and with motion-compensated waveform.

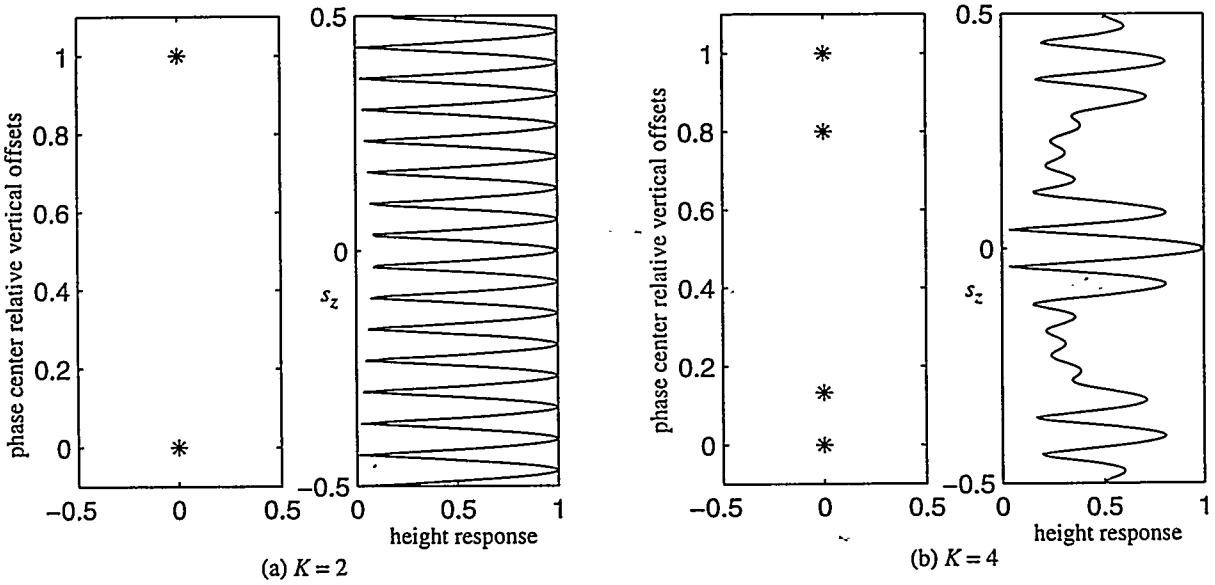

Figure 9. Comparison of height responses vs. antenna effective phase center distributions.

Consider data collected with the real-time motion compensation described by equations (4-6). The collection surfaces would be stacked as in figure 8, and the video phase would be described by

$$\Phi_{video}(i,n,k) \approx \left\{ \frac{4\pi}{c}\left[f_{0,0} + B_{\text{eff},0,0}\left(\frac{i}{I}\right)\right]\cos\psi_{0,0}\left(\begin{array}{c} s_x d\alpha\, n - s_y + s_z\sqrt{1+d\alpha^2 n^2}\tan\psi_{n,0} \\ + s_z \dfrac{\sqrt{1+d\alpha^2 n^2}}{\cos^2\psi_{n,0}}\left(\dfrac{b_{\perp,n,k}}{|r_{c,n,0}|}\right) \end{array} \right) \right\} \tag{18}$$

Reformatting this data to eliminate migration would involve resampling operations to eliminating any cross-coupling of indices i, n, and k. Normal 2-D polar reformatting of each collection plane is completed by resampling in azimuth such that

$$\frac{4\pi}{c}\left[f_{0,0} + B_{\text{eff},0,0}\left(\frac{i}{I}\right)\right]\cos\psi_{0,0} d\alpha\, n \rightarrow \frac{4\pi}{c} f_{0,0}\cos\psi_{0,0} d\alpha\, n'. \tag{19}$$

However, this still leaves substantially non-parallel collection surfaces as previously described. Were it possible, we might consider first resampling the Fourier-domain data in the ω_z direction to the equivalent of new baselines $b'_{\perp,0,k}$, such that

$$\frac{4\pi}{c}\left[f_{0,0} + B_{\text{eff},0,0}\left(\frac{i}{I}\right)\right]\frac{\cos\psi_{0,0}\sqrt{1+d\alpha^2 n^2}}{|r_{c,n,0}|\cos^2\psi_{n,0}} b_{\perp,n,k} \rightarrow \frac{4\pi}{c} f_{0,0}\frac{1}{|r_{c,0,0}|\cos\psi_{0,0}} b'_{\perp,0,k}. \tag{20}$$

We also noted earlier that modulating the baselines on a pulse-to-pulse basis would accomplish much of this, especially for severe squint angles.

In any case, by presuming for the moment that $\sqrt{1+d\alpha^2 n^2}\tan\psi_{n,0} \approx \sqrt{1+d\alpha^2 n'^2}\tan\psi_{n',0}$, the video phase becomes

$$\Phi_{video}(i,n,k) \approx \left\{ \begin{array}{l} s_x\left(\dfrac{4\pi}{c} f_{0,0}\cos\psi_{0,0} d\alpha\, n'\right) - s_y\left(\dfrac{4\pi}{c}\left[f_{0,0} + B_{\text{eff},0,0}\left(\dfrac{i}{I}\right)\right]\right) + s_z\left(\dfrac{4\pi}{c} f_{0,0}\dfrac{1}{|r_{c,0,0}|\cos\psi_{0,0}} b'_{\perp,0,k}\right) \\ + s_z\left(\dfrac{4\pi}{c}\left[f_{0,0} + B_{\text{eff},0,0}\left(\dfrac{i}{I}\right)\right]\cos\psi_{0,0}\sqrt{1+d\alpha^2 n'^2}\tan\psi_{n',0}\right) \end{array} \right\}. \tag{21}$$

Within the brackets, the first line represent the decoupled Fourier samples we want. However, there remain two problems to contend with regarding equation (21).

The first problem is that the expression in the second line represents remaining undesired coupling responsible for layover and height-of-focus perturbations. We note, though, that were it available, an initial estimate of s_z would allow compensating this prior to transforms across indices i and n'. Normal IFSAR processing, however, leaves the resolution of s_z as the final operation, after the transforms across indices i and n'. The second problem is that we have relied upon resampling the baselines, that is, the Fourier-domain data in the ω_z direction. Even with baseline modulation this is somewhat impalpable.

We resolve the first problem by, in fact, processing between collection planes (across k) first. As previously stated, this would allow compensating the offending term. Processing this dimension first also is instrumental in solving the second problem. The natural algorithm then becomes perhaps as follows.

Step 1. Height Transform

We begin by recognizing that what we have are relatively few collection planes, and hence Fourier-domain samples in the ω_z direction. Furthermore, these samples are generally not evenly spaced, and their spacing varies as a function of ω_x and ω_y. An obvious result is that this diminishes both the utility and the need for efficient transform algorithms in this dimension.

We also recognize the applicability of the scale-change property of the Fourier Transform, that states "a linear time-scale change of γ yields a linear frequency-scale change of $1/\gamma$, as well as a spectral magnitude change of $1/|\gamma|$." Consequently, scaling $b_{\perp,n,k}$ prior to a transform is equivalent to scaling the result after the transform. However, in the end, what we really want are stable and uniformly scaled estimates of vertical position s_z.

All these considerations direct us to implementing matched filtering for a common set of s_z at each ω_x and ω_y. That is, we process across collection surfaces in the ω_z direction to multiple but specific layers of s_z, prior to any azimuth or range compression, with the appropriate matched filter changing as a function of indices i and n.

To facilitate eventual s_z peak location, the spacing between s_z layers should be no greater than the nominal lobe width $\rho_z \approx 2\pi/\Delta\omega_z$ due to the largest collection-surface separation. The number of s_z layers should encompass the range of s_z that might be expected for the scene of interest. Depending on ρ_z, this might need to be no more than a small handful of layers, something on the order of perhaps twice the total number of phase wraps due to the widest separated phase centers, from the lowest to highest points in the scene.

Step 2. Data Correction

At this point each layer can be corrected for layover and height-of-focus perturbations. This step also ortho-rectifies the eventual images.

Step 3. Layer Processing

Each s_z layer can now complete 2-D polar format processing in the usual manner.

Step 4. Surface Extraction

The result of the prior processing steps is a data set describing a rectangular parallelepiped in the spatial domain, with dimensions s_x, s_y, and s_z. The a priori presumption that the target scene is a single reflecting surface indicates that but a single valid s_z exists for each s_x, s_y pair. Extracting this surface now amounts to super-resolving a single maximum peak in the s_z direction for each s_x, s_y pair. Clearly, we might advantageously use contextual information and other assistance from adjacent s_x, s_y pairs, as is often done with more typical implementations of IFSAR. Of course, residual ambiguities due to undersampling ω_z for the range of heights in the scene still need to be resolved, as they are manifested as multiple s_z peaks, but this is the same problem as the phase-unwrapping ambiguity in more typical IFSAR.

In this manner, a single height can ultimately be assigned to each horizontal location, resulting in a typical IFSAR product.

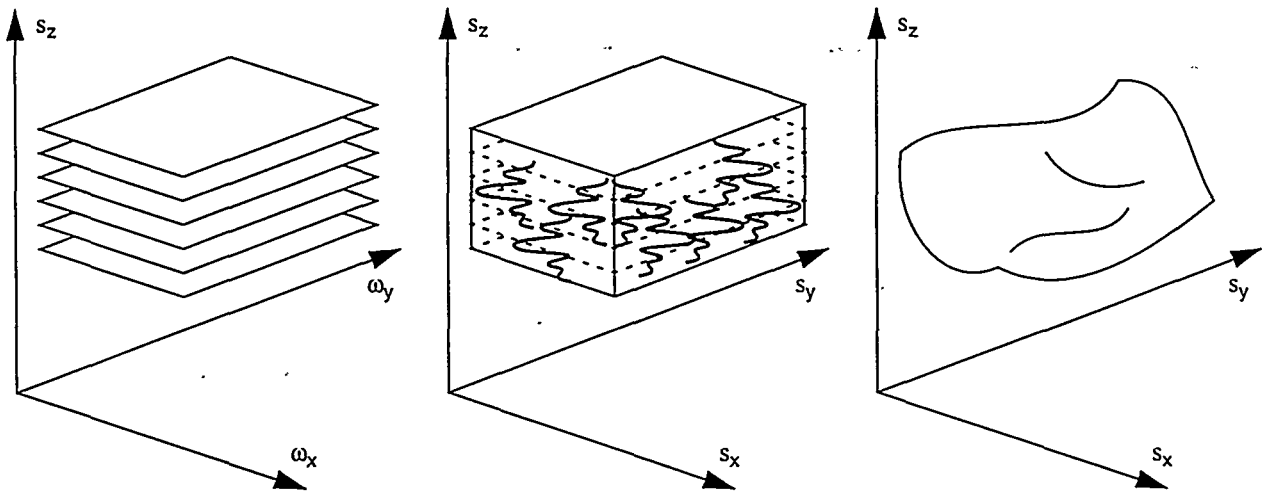

height transformed data
(result of step 1)

spatial domain result
(result of step 3)

extracted surface topography
(result of step 4)

Figure 10. 3-D Polar Format processing steps.

8. CONCLUSIONS

Fundamentally, traditional IFSAR processing is just a degenerate form of 3-D SAR processing (super-resolved and typically undersampled). In so being, several characteristics of the IFSAR data are usually ignored, to the detriment of the final IFSAR product. For example, height migration between typical IFSAR image pairs results in a decorrelation of image pixels. These effects are more severe for fine resolutions, large heights, and severe squint angles. Nevertheless, these effects can be mitigated by approaching the problem from a 3-D SAR perspective, and optimally collecting and/or properly resampling the data in Fourier space, or equivalent. This leads to a 3-D version of the familiar polar format processing algorithm.

Data may be optimally collected by adjusting received frequency and bandwidth on a pulse-to-pulse basis such that the individual collection surfaces in Fourier space all project to the exact same trapezoid on the plane $\omega_z = 0$. Furthermore, the projected baseline length might be adjusted on a pulse-to-pulse basis to stabilize the vertical spatial bandwidth as a function of azimuth collection angle.

Finally, treating IFSAR as a 3-D SAR problem allows easy incorporation of more that two antenna effective phase centers, that is, a multiple baseline geometry.

9. ACKNOWLEDGMENTS

The authors wish to thank Jack Jakowatz, Dan Wahl, and other members of their team for their early constructive comments on this perspective.

Sandia is a multiprogram laboratory operated by Sandia Corporation, a Lockheed Martin Company, for the United States Department of Energy under Contract DE-AC04-94AL85000.

10. REFERENCES

1. Charles V. Jakowatz Jr., Paul H. Eichel, Dennis C. Ghiglia, Paul A. Thompson, *Spotlight-Mode Synthetic Aperture Radar: A Signal Processing Approach*, ISBN 0-7923-9677-4, Kluwer Academic Publishers, 1996.

2. C. V. Jakowatz Jr., D. Wahl, informal memorandum to Armin Doerry, et al., 1 October 1999.

3. Robert N. McDonough, Anthony D. Whalen, *Detection of Signals in Noise* - second edition, ISBN 0-12-744852-7, Academic Press, 1995.

4. Bernard D. Steinberg, *Principles of Aperture and Array System Design*, ISBN 0-471-82102-0, John Wiley & Sons, Inc., 1976.

5. Dennis C. Ghiglia, Daniel E. Wahl, "Interferometric Synthetic Aperture Radar Terrain Elevation Mapping from Multiple Observations", IEEE 6th Digital Signal Processing Workshop, Yosemite National Park, CA, USA, 2-5 Oct. 1994.

6. Wei Xu, Ee Chien Chang, Leong Keong Kwoh, Hock Lim, Wang Cheng Alice Heng, "Phase-unwrapping of SAR Interferogram with Multi-frequency or Multi-baseline", 1994 International Geoscience and Remote Sensing Symposium IGARSS'94, Pasadena, California USA, August 8-12, 1994.

7. Wayne Lawton, "A New Polar Fourier Transform for Computer-Aided Tomography and Spotlight Synthetic Aperture Radar", IEEE Transactions on Acoustics, Speech, and Signal Processing, **Vol. 36**, No. 6, June 1988.